Available online at www.sciencedirect.com
SCIENCE DIRECT
Journal of Power Sources 157 (2006) 260–270
JOURNAL OF POWER SOURCES
www.elsevier.com/locate/jpowsour

Material degradation during isothermal ageing and thermal cycling of hybrid mica seals under solid oxide fuel cell exposure conditions

Yeong-Shyung Chou *, Jeffry W. Stevenson, John Hardy, Prabhakar Singh

K2-44, Materials Division, Pacific Northwest National Laboratory, P.O. Box 999, Richland, WA 99354, USA

Received 27 April 2005; received in revised form 28 June 2005; accepted 10 July 2005
Available online 22 August 2005

Abstract

Hybrid phlogopite mica seals with glass interlayers were evaluated in terms of materials degradation in a combined ageing and thermal cycling test. Three glass interlayers were investigated: a standard Ba–Ca–Al silicate glass (G18), a modified Ba–Ca–Al silicate glass with a nucleation agent added (G18m), and a borosilicate glass (G6). The hybrid phlogopite mica seals were aged at 800 °C for ~500 to ~1000 h in moist, dilute hydrogen fuel, and then subjected to short-term thermal cycling between ~100 and 800 °C. Seals with G18 and G18m glass interlayers showed very poor thermal cycle stability after isothermal ageing. Seals with borosilicate glass interlayers showed very good thermal cycle stability with constant, low leakage (<0.01 sccm cm^{-1} at 0.2 psi) after ageing for 508 h followed by 56 thermal cycles. Post-mortem analyses showed degradation of the mica due to interaction with the interlayer glasses. Leak paths were identified and correlated to the measured leak rates.

Keywords: Ageing; Thermal cycling; Leak rate; Mica seal; Phlogopite; SOFC

1. Introduction

It is recognized that sealing of solid oxide fuel cell (SOFC) stacks is one of the most challenging tasks for advancing SOFC technologies. The sealant or sealants have to survive numerous thermal cycles in the harsh SOFC environments, i.e., both oxidizing and reducing atmospheres at elevated temperatures. Stationary applications may require hundreds of thermal cycles, while transportation applications may require thousands of cycles. In addition to maintaining low leak rates during repeated thermal cycles, the sealants also have to exhibit long-term (>40,000 h) mechanical, thermal, chemical, and electrical stability during SOFC operation.

There are several different approaches to SOFC seal development, including rigid glass and/or glass-ceramic seals [1–4], compressive seals [5–7], and brazes [8]. Each approach has its own advantages as well as disadvantages [2,7,8]. In this paper we report recent progress in the development of compressive mica seals. In earlier studies, we identified the major leak paths of conventional compressive mica seals to be at the interfaces between the mating materials and the mica seal, not through the mica seal itself [5,6]. Based on the findings, a "hybrid" mica seal was developed which included the addition of two extra interlayers at these interfaces (Fig. 1). The high temperature leak rates for these seals were reduced by two to three orders of magnitude as compared to the conventional mica seal [5,6]. The seals were also found to have reasonable thermal stability in air or a moist reducing environment [9]. Moreover, the seals demonstrated excellent thermal cycle stability over 1026 thermal cycles from ~100 to 800 °C in a moist reducing environment. Nevertheless, the issue of long-term stability remained to be investigated. In addition, a more critical issue is the effect of combined ageing and thermal cycling in dual atmospheres on the integrity of the seals, especially regarding materials interaction or degradation at the interface or in the mica itself. In this paper, we report the high temperature leakage of hybrid phlogopite mica seals with three different glass interlayers during combined ageing at 800 °C and short-term thermal cycle testing. Post-test

* Corresponding author. Tel.: +1 509 375 2527; fax: +1 509 375 2186.
E-mail address: yeong-shyung.chou@pnl.gov (Y.-S. Chou).

0378-7753/$ – see front matter © 2005 Elsevier B.V. All rights reserved.
doi:10.1016/j.jpowsour.2005.07.027

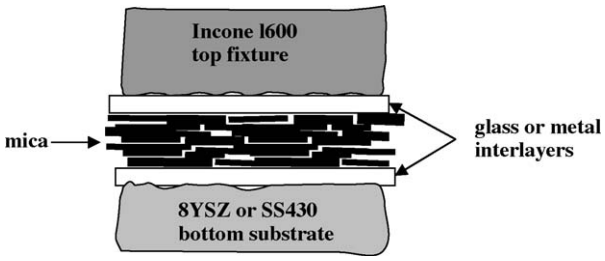

Fig. 1. Schematic showing the cross-section view of the structure of the hybrid phlogopite mica seal. Phlogopite mica paper is sandwiched between two glass interlayers. In comparison, a conventional compressive mica seal does not have the interlayers.

analyses were also performed to characterize the degradation and failure of the hybrid micas.

2. Experimental

2.1. Interlayer glass preparation

In this study, three glasses, designated G18, G18m, and G6, were tested as the interlayer glass of the hybrid mica seal design. The nominal chemical compositions of the glasses are listed in Table 1. G18 is a standard Ba–Ca–Al silicate (BCAS) sealing glass developed at the Pacific Northwest National Laboratory for solid oxide fuel cell sealing applications [10]. The glass was made by mixing the constituent oxides in reagent grades and melting at ~1500–1550 °C. After melting, it was quenched, crushed, and attrition milled with zirconia media in *iso*-propanol for 2 h. The glass powders were then dried in an oven (~110 °C) for several hours. Glass G18m was a modified G18 glass made by mixing of 5 wt.% TiO_2 powder (Rutile, 99.5% Alfa Aesar, MA) with the G18 glass powder. The addition of TiO_2 powders was intended to promote crystallization to minimize interactions between the mica and glass. Glass G6 was a commercial low melting temperature borosilicate glass in the form of filter paper (Fisher Scientific, glass fiber circle cat# 09-804-110A). It contained slightly more B_2O_3 (9.6 wt.%) than G18 glass (7.2 wt.%), and high alkali content (Table 1). This glass was chosen based on its availability in thin paper form (~150–250 μm) and absence of binders for easy application in hybrid mica seal tests. Glass G6, which served in this study as a reference non-crystallizing glass (to contrast with the readily crystallized G18 and G18m glasses), was found to have good wetting on Inconel600 and 8YSZ materials in earlier studies of thermal cycling and leakage [5,9].

Table 1
Glass compositions (wt.%) and thermal properties after heat-treatment

	Glass#		
	G18	G18m	G6
BaO	55.6	52.9	4.5
CaO	8.7	8.3	2.6
Al_2O_3	5.3	5.0	6.3
B_2O_3	7.2	6.9	9.6
SiO_2	21.8	20.7	58.7
K_2O			3.2
TiO_2		4.7	
Na_2O			11.1
ZnO			3.5
ZrO_2	1.5	1.4	0.4
T_g (°C)	554	553	538
T_s (°C)	837	832	599
CTE (ppm °C^{-1})	12.4	11.7	9.4

2.2. Thermal and microstructure characterization

The three glass materials were characterized in terms of thermal properties and crystalline phases. Differential thermal analysis (DTA) was conducted to determine the glass transition point (T_g) and crystallization temperature (T_c). Thermal gravimetric (TG) analysis was also conducted. The analyses were performed in air on powder samples (<#325 mesh) for G18 and G18m glasses. For glass G6, the as-received filter paper form was used without grinding into powder form. The DTA/TG equipment was a Netzsch STA449C; the heating rate was 5 °C min^{-1}. The linear thermal expansion coefficient (CTE) and T_g were determined by dilatometric measurement (Unitherm model 1161, Anter Corp., PA) of sintered bars (about 25 mm long). The G18 and G18m CTE samples were made by cold pressing the glass powders at ~50 MPa, followed by sintering at 850 °C for 1 h and 750 °C for 4 h in air. The G6 CTE bar was made by sintering the as-received glass fiber paper in a stack to 800 °C for 1 h followed by 750 °C for 4 h. After sintering, the CTE samples were cut into the desired dimensions for measurement. Sintered samples were also used for microstructure characterization by scanning electron microscopy (JEOL, JSM-5900LV). Crystalline phase characterization of sieved powders (<#325 mesh) was performed by X-ray diffraction (XRD) analysis using Cu Kα radiation with a step size of 0.05° 2θ and 1 s count (Philips Electronic Instruments, Model XRG3100 X-ray generator with Wide Range Vertical Goniometer).

2.3. Mica and hybrid seal assembly

The mica used in this study was a commercially available phlogopite mica paper with a thickness of about 100–200 μm (ultra-high temperature mica, cat# 85955K21, McMaster-Carr, GA). Phlogopite mica was selected due to its higher thermal stability and CTE compared to muscovite micas [7]. The mica paper was composed of large, overlapping discrete mica flakes (hundreds to a thousand microns in size) with ~5 wt.% of organic binder. For the combined ageing and thermal cycling tests, the phlogopite mica paper (2 in. × 2 in.) was sandwiched between two glass interlayers to form a "hybrid" mica seal [1,2]. The hybrid mica assembly was then pressed between an Inconel600 fixture and a flat substrate of

dense 8YSZ, as-received 430 stainless steel (SS430) or oxide-coated 430 stainless steel (CT430) as shown in Fig. 1. Glass interlayers of G18 and G18m were made by conventional tape casting of the glass powders in an organic solvent system [10]. The thickness of the green glass tape was about 200 μm. Glass interlayers of G6 were made from the as-received filter paper form.

2.4. High temperature leak tests during isothermal ageing and thermal cycling

The high temperature leak rate was measured with ultra-high purity helium and was determined by monitoring the pressure change of a known volume with time. The details of the leak rate calculation and experimental setup are given in Refs. [5,6]. In the current test, the pressure for leak tests across the hybrid mica seal was 0.2 psi. For the combined ageing and thermal cycling tests, the hybrid mica samples were first aged at 800 °C for about 500–1000 h, followed by short-term thermal cycling between ~100 and 800 °C. The temperature profiles for the thermal cycling are given in Refs. [11,12]. During the tests (except when conducting the leak test), a fuel of ~2.7% H_2/bal. Ar was passed through the inside of the sealed fixture at a constant rate of 30 sccm (the outside of the seal was exposed to ambient air). The fuel was bubbled through water to add ~3% H_2O to simulate the wet and reducing SOFC anode environment. After the test, the mica samples were detached from the test fixture and characterized with optical and scanning electron microscopy. For comparison, a hybrid mica seal with G18 glass interlayers was subjected to short-term thermal cycling only (without isothermal aging) under the same conditions to differentiate the effects of constant temperature ageing on materials degradation and microstructure evolution.

3. Results and discussion

3.1. Differential thermal analysis (DTA) and thermal gravimetric analysis (TGA)

The DTA traces for the three glasses are shown in Fig. 2. For glass G6, a weak glass transition point (T_g) appeared to occur around 580 °C. The peak temperature at ~640 °C corresponded to the melting of the glass fibers in the filter paper, rather than the onset of crystallization. Glasses G18 and G18m both showed very similar DTA traces with T_g of 560 °C for glass G18 and T_g of 562 °C for glass G18m. The two broad peaks at around 689 and 910 °C may correspond to separate crystallization events. The addition of small amount of TiO_2 powders into G18 powders appeared to have minimal effect of the crystallization of the G18 glass. Thermal gravimetric analyses (not shown here) of the three glasses all showed nearly constant weight with less than 0.25% of weight loss during the analysis.

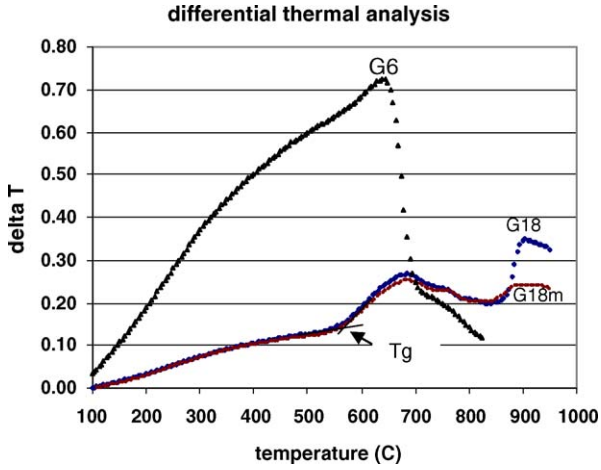

Fig. 2. Differential thermal analysis of G18, G18m, and G6 glasses. G18 and G18m were tested in powder form, and G6 was tested in the as-received filter paper form. Samples were heated at 5 °C min^{-1} in air.

3.2. Dilatometry measurements

The measured linear thermal expansion curves of the three sintered glasses are shown in Fig. 3, together with the glass transition point (T_g) and the softening point (T_s). The glass transition points for the three heat-treated glasses are 538 °C for glass G6, 554 °C for glass G18, and 553 °C for glass G18m, consistent with the DTA results for glasses G18 and G18m. The glass softening points for the three heat-treated glasses are 599 °C for glass G6, 837 °C for glass G18, and 832 °C for glass G18m. Glass G6 retained its glassy structure and softened at 599 °C, while glasses G18 and G18m experienced significant crystallization although they still contained some residual glass which softened at 832–837 °C. The average coefficient of thermal expansion (CTE) from room temperature to the glass transition point of the three heat-treated glasses was 9.4×10^{-6} °C^{-1} for glass G6, 12.4×10^{-6} °C^{-1}

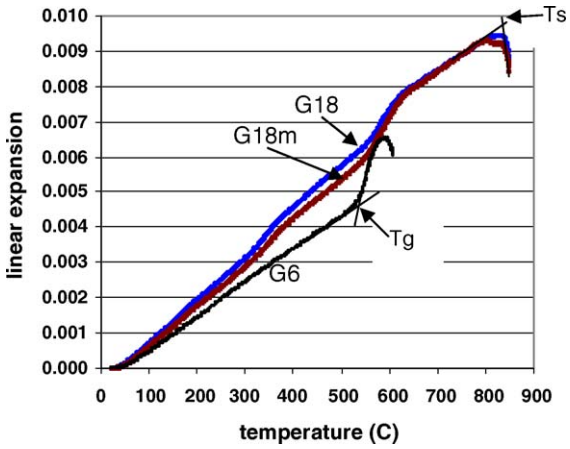

Fig. 3. Linear thermal expansion of heat-treated G18, G18m, and G6 glasses. G18 and G18m were treated at 850 °C/1 h followed by 750 °C/4 h. G6 was treated at 800 °C/1 h followed by 750 °C/4 h.

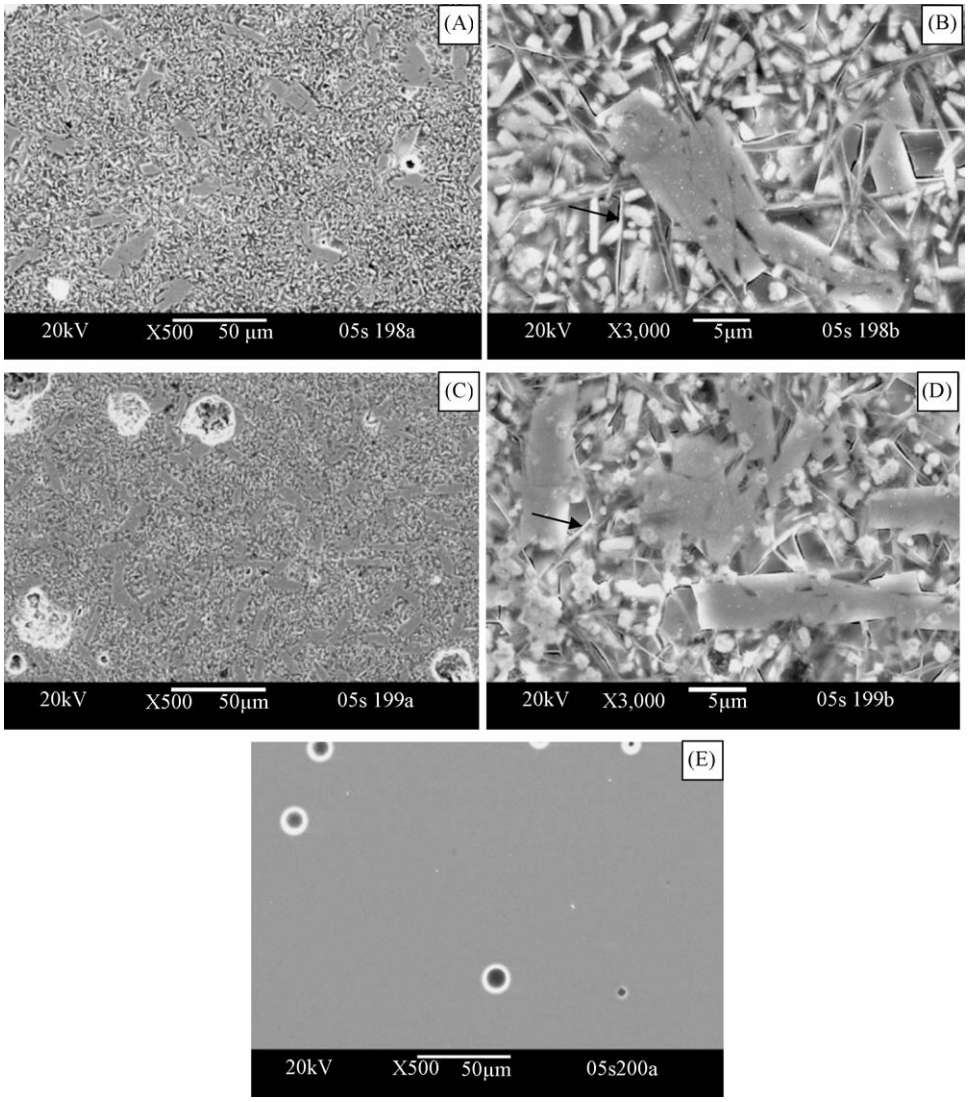

Fig. 4. Microstructure development of the three glasses: (A) and (B) are low and high magnifications of G18, (C) and (D) are low and high magnifications of G18m, and (E) is a low magnification of glass G6. Glasses G18 and G18m were heat treated at 850 °C/1 h followed by 750 °C/4 h. Glass G6 was heat treated at 800 °C/1 h followed by 750 °C/4 h.

for glass G18, and $11.7 \times 10^{-6}\,^{\circ}C^{-1}$ for glass G18m. The slightly lower CTE of G18m is likely due to the presence of less $BaSiO_3$ (or more $BaAl_2Si_2O_8$, $BaSiO_3$ has a higher CTE than hexa-celsian, $BaAl_2Si_2O_8$) in the crystallized G18m, as discussed in the next section.

3.3. Microstructure and phase characterization

The microstructures of the three glasses after heat treatment are shown in Fig. 4. It is clear that both G18 and G18m were substantially crystallized, with very similar microstructures consisting of $BaSiO_3$ rods a few microns in size (light phase) and much larger (15–25 μm) elongated hexa-celsian $BaAl_2Si_2O_8$ grains (darker phase). Both glass also contained small amount of a fibrous phase containing Ba, Ca, Al and Si (arrows in Fig. 4B and D) as well as residual glass. Overall, G18m appeared to have a higher fraction of the hexa-celsian phase (or less $BaSiO_3$). In contrast, the glass G6 remained vitreous without distinct microstructural features (Fig. 4E). The heat-treated glasses were also characterized with X-ray powder diffraction. The XRD patterns are shown in Fig. 5. It is evident that the heat-treated glasses G18 and G18m had very similar crystalline phases. Major phases were $BaSiO_3$ and hexa-celsian ($BaAl_2Si_2O_8$); minor amounts of Al_2SiO_5 and $Ca_2BaSi_3O_9$ also appeared to be present. Glass G18m, to which TiO_2 was added may also have contained small amounts of $Ba_2TiSi_2O_8$. In the barium aluminosilicate system, there are three polymorphic forms of celsian phase: monoclinic celsian, hexagonal (hexa-celsian), and orthorhombic (paracelsian). Monoclinic celsian is stable from room temperature up to 1590 °C; above this temperature hexa-celsian is stable up to the melting point (1760 °C). However, glasses normally crystallize as metastable hexa-celsian even below 1590 °C [14], as was observed in this

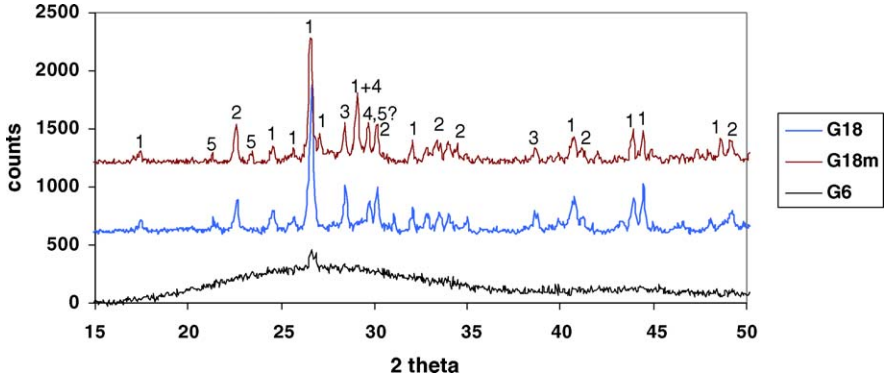

Fig. 5. XRD patterns of the heat treated G18, G18m, and G6 glasses. G6 appears to be primarily amorphous with a minor quartz peak. G18 and G18m have similar crystalline phases of $BaSiO_3$ (marked by 1), $BaAl_2Si_2O_8$ (2), and Al_2SiO_5 (3). G18m may also contains $Ba_2TiSi_2O_8$ (4) and/or $Ca_2BaSi_3O_9$ (5).

study. The conversion from the hexagonal to the monoclinic polymorph is feasible but the transformation is very sluggish [15]. From an SOFC sealing point of view, the metastable hexagonal celsian phase is preferred because it has a higher CTE of $8 \times 10^{-6}\,^{\circ}C^{-1}$ than that of the monoclinic celsian ($3 \times 10^{-6}\,^{\circ}C^{-1}$) [16]. The very low CTE of monoclinic celsian phase could lead to undesirable microcracking or cracking during the routine operation of thermal cycling of SOFC stacks.

3.4. Leak rates of hybrid mica seal with G18 glass interlayers during isothermal ageing and thermal cycling

The normalized leak rates (in standard cubic centimeter per minute per unit leak length of seal perimeter, sccm cm^{-1}) of the hybrid phlogopite mica seal with G18 glass interlayers are shown in Fig. 6. The seal was pressed between an Inconel600 fixture and a dense 8YSZ electrolyte plate at a low applied compressive stress of 6 psi. This couple offered a large CTE mismatch (CTE of Inconel600 is $16–17 \times 10^{-6}\,^{\circ}C^{-1}$ and that of 8YSZ is $10.5 \times 10^{-6}\,^{\circ}C^{-1}$). Fig. 6A shows the 800 °C leak rate during the constant temperature ageing and Fig. 6B shows the leak rate during the subsequent short-term thermal cycling between ~100 and 800 °C. In Fig. 6A, the leak rate remained fairly constant at ~0.02 sccm cm^{-1} during the initial ageing up to about 350 h. The leak rate then dropped substantially to about $(1–2) \times 10^{-3}$ sccm cm^{-1}, close to the current detection limit of 1×10^{-3} sccm cm^{-1}. The leak rate, however, jumped rapidly to about 0.04 sccm cm^{-1} after ageing for about 850 h and remained fairly constant until 1036 h when the thermal cycling tests were started. During the subsequent thermal cycling (Fig. 6B), the leak rates gradually increased from ~0.04 to ~0.09 sccm cm^{-1}, and then rapidly increased to ~0.32 sccm cm^{-1} after 21 thermal cycles, which is equivalent to leak rates observed for failed rigid glass seals during thermal cycling. For comparison, a hybrid mica seal with G18 glass interlayers was also tested with thermal cycling only (i.e., without the preliminary isothermal ageing at 800 °C). The leak rates versus the number of thermal cycles for that test are shown in Fig. 7. The initial leak rates were ~0.02 sccm cm^{-1}, in good agreement with the initial leak rates of the aged sample, i.e., 0.018–0.023 sccm cm^{-1} in Fig. 6. The leak rates increased to ~0.05–0.06 sccm cm^{-1}

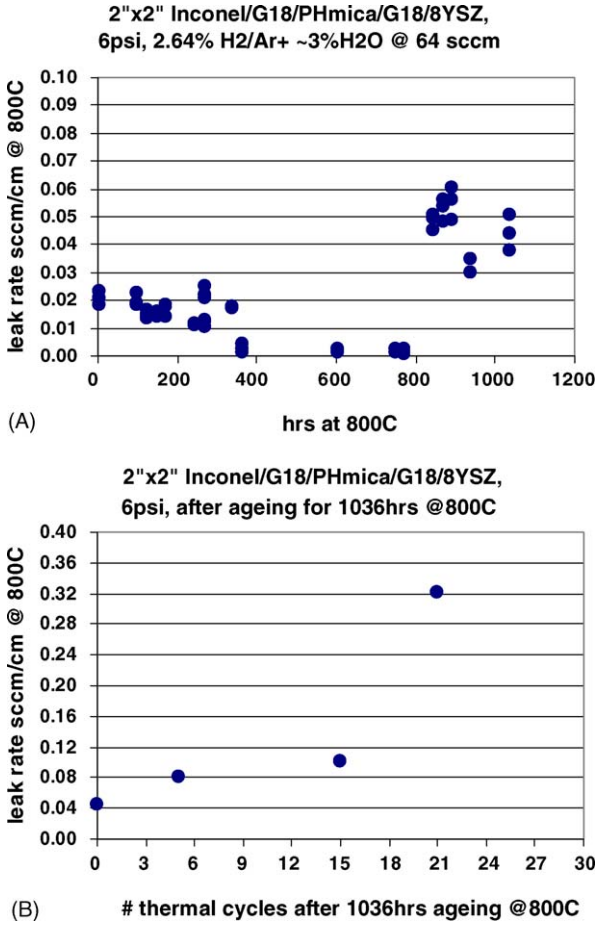

Fig. 6. (A) Normalized leak rate of a hybrid phlogopite mica seal with G18 glass interlayers during isothermal ageing at 800 °C in a flowing reducing environment of ~2.7% H_2/bal. Ar + ~3% H_2O. The mica sample was pressed between an Inconel fixture and an 8YSZ plate at 6 psi. (B) Normalized leak rate of the hybrid mica seal during thermal cycling after ageing for 1036 h at 800 °C.

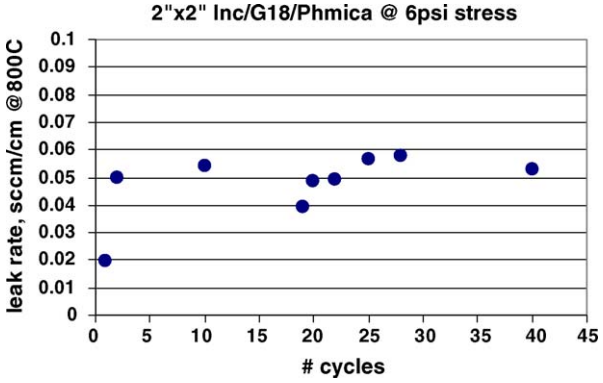

Fig. 7. Normalized leak rate of a hybrid phlogopite mica seal with G18 glass interlayers during thermal cycling in a flowing reducing environment of ~2.7% H_2/bal. Ar + ~3% H_2O. The mica sample was pressed between an Inconel fixture and an alumina plate at 6 psi. Note that this sample was thermally cycled without prior isothermal ageing at 800 °C.

after initial thermal cycles but remained constant during the following 40 thermal cycles. It is clear that the aged and thermally cycled sample behaved differently from the sample that was only thermally cycled. The difference between the two samples and the change in leak rates during ageing was attributed to reaction of interlayer glass with the phlogopite mica and is discussed below.

3.5. Leak rates of hybrid mica seal with G18m glass interlayers during ageing and thermal cycling

The normalized leak rates of the hybrid phlogopite mica seal with G18m glass interlayers are shown in Fig. 8. Note that this sample was pressed between an Inconel600 fixture and an oxide-coated stainless steel 430 (SS430) plate at the same compressive stress of 6 psi. Stainless steel 430 is a ferritic steel which has a very good CTE match (CTE = 12.5 ppm °C^{-1}) with Ni/YSZ anode-supported cells [13]. Fig. 8A shows the 800 °C leak rate during the isothermal ageing, and Fig. 8B shows the leak rate during the subsequent thermal cycling. In Fig. 8A, it is evident that the leak rate remained constant at ~0.02 sccm cm^{-1} during the entire ageing period of 1036 h. During the subsequent thermal cycling (Fig. 8B), however, the leak rate increased rapidly from ~0.02 to ~0.16 sccm cm^{-1} after six thermal cycles. The possible

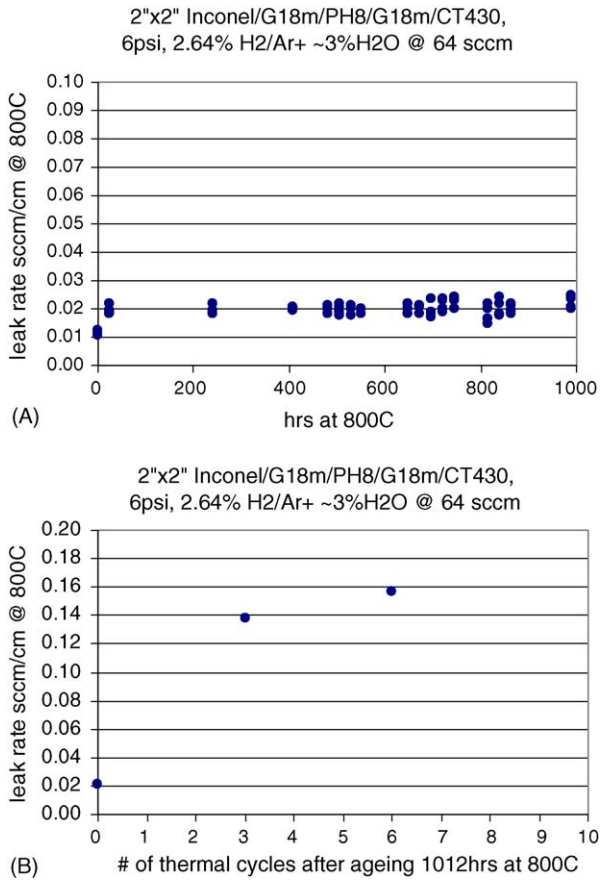

Fig. 8. (A) Normalized leak rate of a hybrid phlogopite mica seal with G18m glass interlayers during isothermal ageing at 800 °C in a flowing reducing environment of ~2.7% H_2/bal. Ar + ~3% H_2O. The mica sample was pressed between an Inconel fixture and an oxide-coated SS430 (CT430) plate at 6 psi. (B) Normalized leak rate of the hybrid mica seal during thermal cycling after ageing for 1036 h at 800 °C.

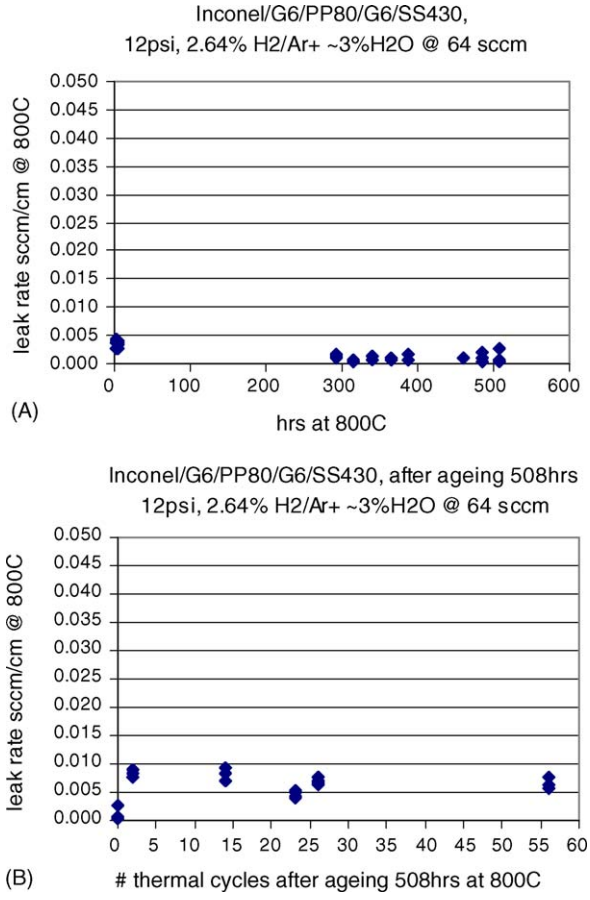

Fig. 9. (A) Normalized leak rate of a hybrid phlogopite mica seal with G6 glass interlayers during isothermal ageing at 800 °C in a flowing reducing environment of ~2.7% H_2/bal. Ar + ~3% H_2O. The mica sample was pressed between an Inconel600 fixture and an as-received SS430 plate at 6 psi. (B) Normalized leak rate of the hybrid mica seal during thermal cycling after ageing for 508 h at 800 °C.

cause of the abrupt increase in leak rate during short-term thermal cycling is discussed below.

3.6. Leak rates of hybrid mica seal with G6 glass interlayer during isothermal ageing and thermal cycling

The leak rates of the hybrid mica seal with G6 borosilicate glass interlayers are shown in Fig. 9. Note that this sample used a thinner phlogopite mica paper (about 50–56 μm thick as compared to about 220–230 μm for the previous two samples) and an uncoated stainless steel 430 plate at the same compressive stress of 6 psi. In this test, the thinner mica and low melting glass (G6) were used to see if degradation occurred more rapidly through thinner mica paper, and the isothermal ageing was stopped at ~500 h. Fig. 9A shows the 800 °C leak rate during the isothermal ageing, and Fig. 9B shows the leak rate during the subsequent thermal cycling. In Fig. 9A, the measured leak rate was ~0.001 to ~0.004 sccm cm^{-1} and remained fairly constant during the entire ageing period of 508 h. It is evident that the leak rate was much smaller than for the other two samples in which the mica paper thickness was about four to five times greater. This is consistent with a previous study of the effect of mica thickness on leak rate during thermal cycling, in which higher leak rates were observed for thicker micas than for thinner micas [12]. Given the fact that the total leak through mica is driven by Darcian flow due to the pressure gradient plus bulk diffusion driven by concentration gradients across the mica, the leak rate should be proportional to the cross-sectional area of open channels between mica flakes.

Since the thinner mica had a cross-sectional open area about four to five times less than the thicker micas, it is not surprising that the leak rates for the thinner seal were also about four to five times lower. The initial leak rates of the thicker micas before ageing were about 0.01–0.02 sccm cm^{-1} (Figs. 6A and 8A). The initial leak rates for the thinner mica were about 0.004 sccm cm^{-1}. During the subsequent thermal cycling, the leak rates increased to ~0.005 to ~0.009 sccm cm^{-1} and remained fairly constant during the 56 thermal cycles.

3.7. Fracture surface and microstructure analysis

After the tests, all samples were easily detached from the test fixtures, with fracture occurring along or near the interface with the Inconel600. This was expected due to the larger CTE mismatch between the hybrid mica/glass seal and Inconel600 compared to the bottom substrate. A fracture surface of the hybrid mica seal with G18 glass interlayers after aging (800 °C/1036 h) and thermal cycling (21 cycles) are shown in Fig. 10A (low magnification) and Fig. 10B (high magnification). Note the compressed regions are within the

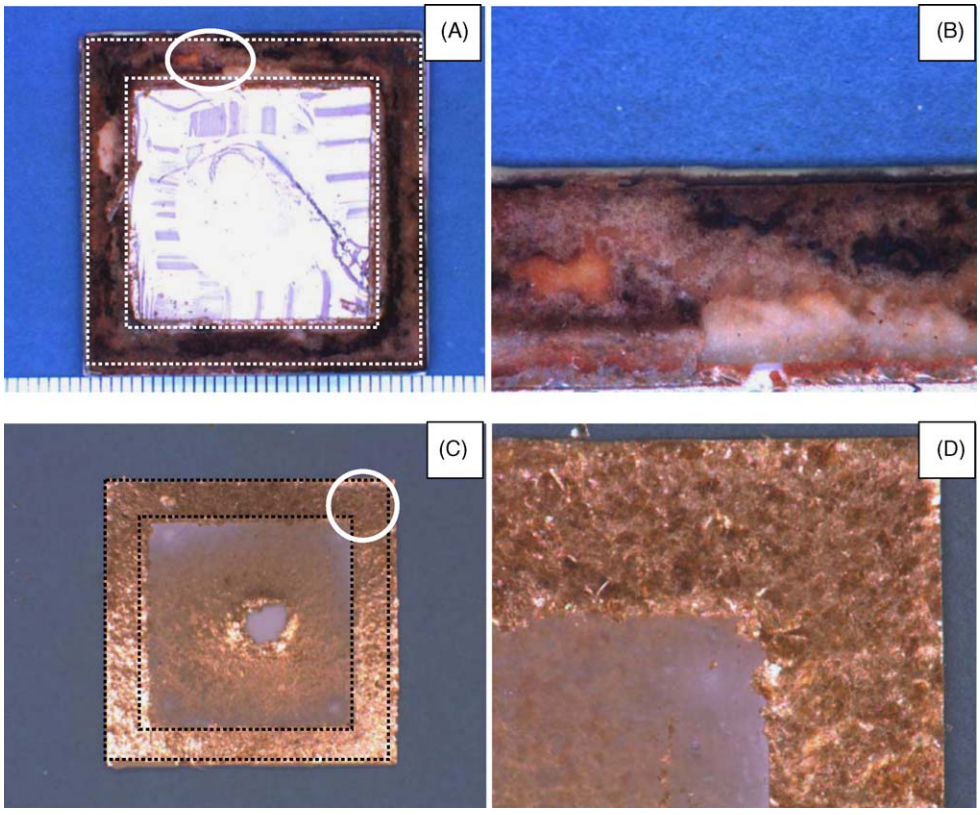

Fig. 10. Fracture surface of hybrid mica seals with G18 glass interlayers: (A) the seal which was aged (800 °C/1036 h) and thermally cycled; (C) the seal which was thermally cycled without preliminary aging. Note that the mica was compressed between the dotted lines during the test. (B) and (D) are higher magnifications of the circled region of the aged and simple cycled samples, respectively.

dotted lines in these photos. For comparison, a fracture surface of the seal that was thermally cycled (40 cycles) without ageing is shown in Fig. 10C (low magnification) and Fig. 10D (high magnification). It is evident that the aged mica sample reveals non-homogeneous color on the fracture surface (Fig. 10A and B). The fracture surface shows no trace of intact mica flakes which appear shiny and reflective under optical microscopy, as observed on the sample that was only thermally cycled (Fig. 10D). The absence of intact mica flakes on the fracture surface clearly indicated some degradation of the phlogopite mica.

Fig. 11A shows a cross-section of the aged and thermally cycled hybrid mica seal with G18 glass interlayers where the fracture occurred along the Inconel600 side. Fig. 11B is a higher magnification of the circled area in Fig. 11A. Fig. 11C shows the fracture surface morphology with bi-modal pore distributions, large pores with diameter in the range of ~100 to ~400 μm, and small pores with diameter in the range of ~5 to ~20 μm. It is evident that the discrete phlogopite mica flakes were transformed into a dense monolithic material with white boundaries at either side (arrows in Fig. 11B). Chemical compositions as determined by energy dispersive spectroscopy on circled areas 1, 2, and 3 in Fig. 11B are listed in Table 2 (note that boron could not be detected by the instrument). The elemental analyses of the mica and G18 glass are also listed. It is clear that the discrete phlogopite mica flakes reacted with G18 glass (Ba–Ca–Al silicate) to form a monolithic material. The reaction of glass with mica was evident by the fact that Ba (from the G18 glass) was present throughout the whole mica region. The two white regions at the boundaries of the reacted mica had the highest Ba content (~22 at.%). The Ba content gradually decreased to ~10 at.% in circled region 2 and to ~8 at.% in circled region 3. It was interesting to note that neither region 1 nor region 2 contained detectable K which suggested these two regions were crystalline in structure rather than glassy phases. In contrast, region 3 has more K than the original phlogopite mica (Table 2). It is likely that the outer mica flakes reacted with the molten sealing glass at the contact boundaries in the early stage of the ageing process, and crystallized into Ba–Mg oxide silicate (likely $BaSiO_3$ and $MgSiO_3$). As the ageing progressed, the residual glass containing Ba, B, and

Table 2
Elemental analysis (in at.%) of circled areas 1, 2, and 3 in Fig. 11 of the hybrid mica seal with G18 glass interlayer after ageing and thermal cycling

Element	Area #1	Area #2	Area #3	Free mica	G18
OK	45.41	48.10	47.20	54.00	52.60
FK	–	–	–	–	–
MgK	7.98	8.95	8.34	13.31	–
AlK	–	9.63	8.10	6.25	5.77
SiK	22.49	20.77	18.88	18.81	17.90
KK	–	–	7.03	5.76	–
CaK	1.38	–	1.30	–	6.17
FeK	0.92	2.26	1.64	1.61	–
BaL	21.82	10.29	7.50	0.25	17.55

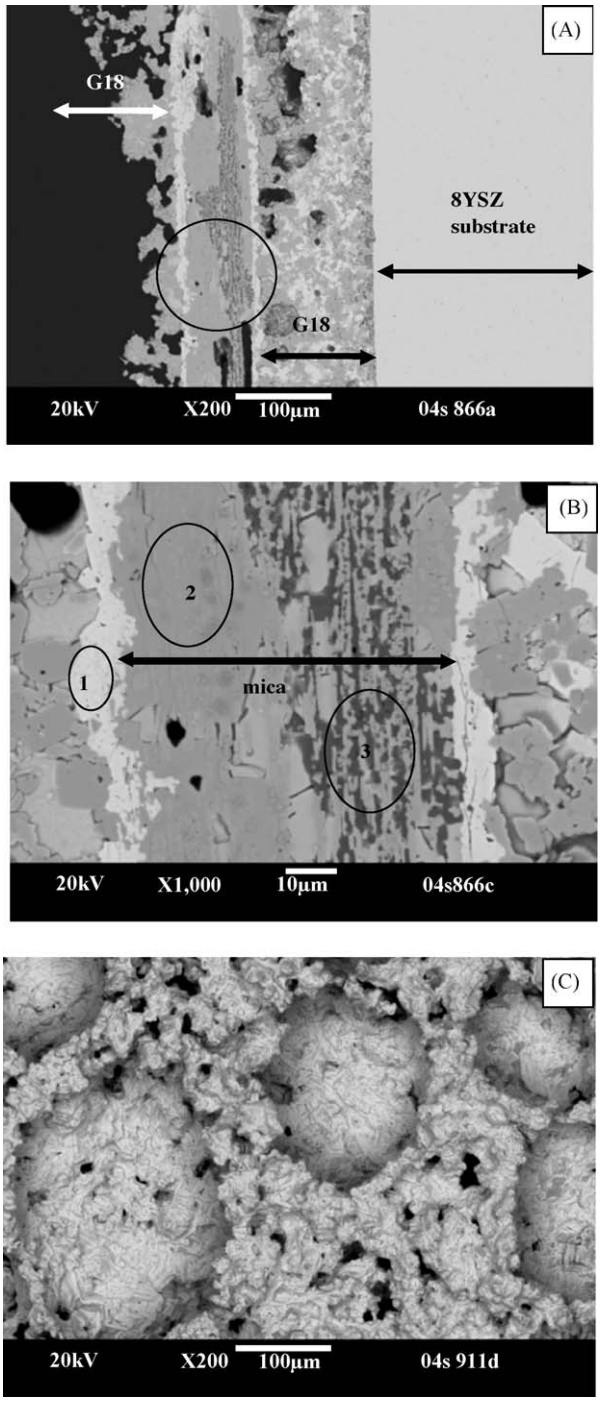

Fig. 11. Cross-section view of the hybrid phlogopite mica seal with G18 glass interlayer after ageing and thermal cycling: (A) an overall view and (B) a higher magnification of the circled region in (A). (C) is a SEM micrograph of the fracture surface. Chemical analyses were conducted with EDS on circled areas 1, 2, and 3 in (B) and the results are listed in Table 2.

K and other elements continued reacting inwards throughout the entire thickness. This degradation process is likely time-dependent and appears to be consistent with the high temperature leak rate data in Fig. 6A in that the leak rate gradually decreased to the detection limit of the current leak setup at about 360 h of ageing. For comparison, the sample

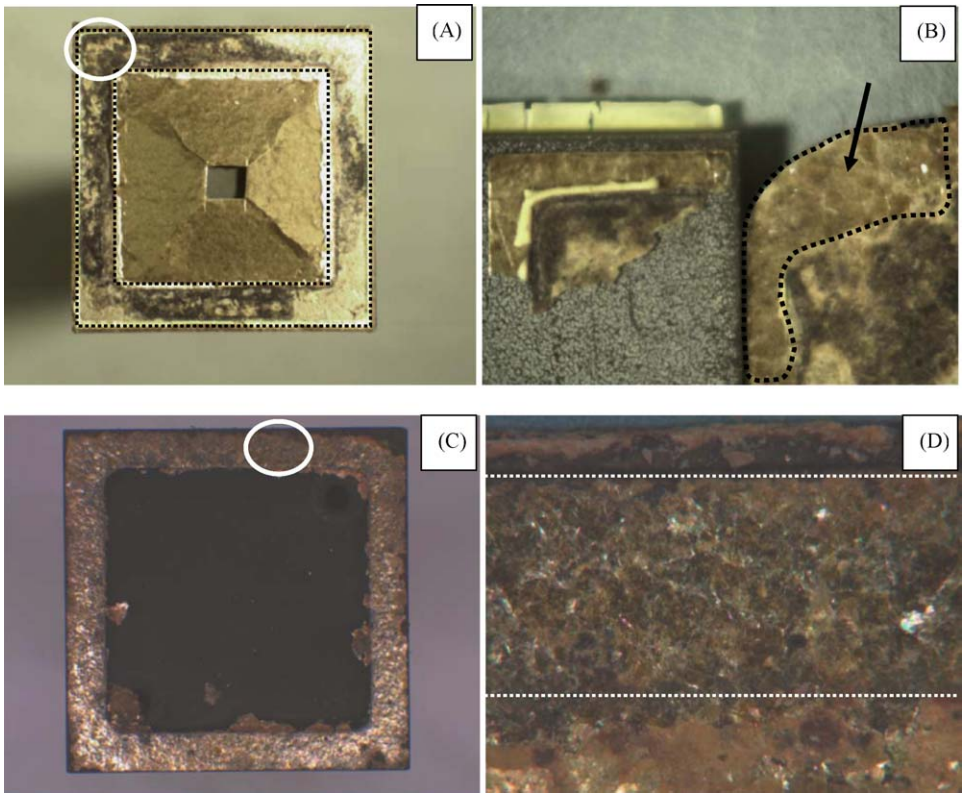

Fig. 12. Fracture surface of the aged and thermally cycled hybrid mica seals with G18m (A) and G6 (C) glass interlayers. Note that the mica was compressed between the dotted lines during the test. (B) and (D) are higher magnifications of the circled region of the mica samples with interlayers of glass G18m and G6, respectively. The hybrid mica seal with G18m glass interlayers show no intact mica flakes on the fracture surface; however, intact mica flakes were present underneath the fracture surface (dotted region). The hybrid mica seal with the G6 glass interlayers showed intact mica flakes.

that was thermally cycled without isothermal aging showed a fairly constant leak rate over 40 thermal cycles (Fig. 7). The total cumulative ageing time in that test was only 80 h (2 h at 800 °C per thermal cycle for a total of 40 cycles). Therefore the degradation or reaction was not complete through the whole mica thickness (∼100 μm), and intact mica flakes remained in the seal, as observed at the fracture surface (Fig. 10D).

As shown in Fig. 6A, the leak rates of the seal with G18 glass interlayers eventually jumped to ∼0.04 sccm cm^{-1} after remaining at the detection limit of ∼0.001 sccm cm^{-1} from ∼360 to ∼800 h during the 800 °C ageing. The sudden increase in leak rate was likely due to linkage of some large pores and small pores (Fig. 11C) to form a continuous leak path. The formation of large pores in this sample was likely due to the release of crystalline water from the phlogopite mica flakes during their reaction with G18 glass. Note that the phlogopite mica could lose up to about 5 wt.% of water from the hydroxyl groups associated with the structure. The water trapped within the pores would likely contribute to hydrostatic tensile stresses and stress corrosion of the silicate glass. As a result, the gaseous water may have eventually cracked open leak paths between pores leading to a much higher leak rate. If this mechanism is correct, it is not surprising that the leak rate remained fairly constant once the trapped water was released. It is interesting to note that the leak rate remained relatively small compared to leak rates typical of fractured rigid seals. This may be because the two newly formed fracture surfaces remained closely matched with each other under the applied stresses, whereas rigid glass seals are usually not operated under an applied compressive stress. The closely matched fracture surfaces were quickly lost during the following thermal cycles as grains on the fracture surfaces were pulled-out, micro-fractured, and reoriented due to anisotropy in CTE so that the crack openings (leak paths) likely increased with each thermal cycle. This is consistent with the observed behavior during thermal cycling as the leak rate eventually jumped to 0.32 sccm cm^{-1} (Fig. 6B). It needs to be pointed out that the common features of typical brittle fracture, i.e., mirror, mist, and especially hackle lines on glass or monolithic ceramics [17] were not retained during the repeated thermal cycling due to grain boundary grooving effects. This prevented the identification of the critical flaw that led to the failure.

The fracture surfaces of the aged and thermally cycled hybrid mica seals with glass G18m and G6 as the interlayers are shown in Fig. 12A and C, respectively. Higher magnification of the circled regions are shown in Fig. 12B and D. It is evident that the aged and thermally cycled seal with G18m glass did not exhibit intact mica flakes on the frac-

ture surface, but the seal with glass G6 did. The fracture of the hybrid seal with glass G18m appeared to occur through different paths, i.e., the bright region and the dark region in Fig. 12A. The bright region was the fracture through the interlayer glass itself, and the dark region was the fracture near the interface between Inconel600 and G18 glass. The fracture near the Inconel600/G18 interface was expected since the largest CTE mismatch was present near that interface. The fracture through the interlayer glass G18m might be related to microstructure defects. Although the fracture surface of the hybrid mica seal with G18m interlayers (Fig. 12A and B) showed no intact mica flakes (similar to the hybrid mica seal with G18 glass (Fig. 10A and B)), the leak rate during ageing was much different as the leak rate remained almost constant during the entire 1000 h of ageing (Fig. 8A). Upon careful peeling off of the top glass interlayers, intact mica flakes were revealed (dotted region in Fig. 12B), indicating that the mica flakes did not react completely with glass G18m to form a monolithic body. Therefore, the leak path remained unchanged, i.e., through the discrete mica flakes, during the ageing process and constant leak rates were obtained.

It is interesting to note that the addition of 5% TiO_2 to the G18 glass to form G18m apparently retarded the rate of glass/mica reaction. For common glass-ceramics, a nucleation agent like TiO_2 and ZrO_2 is often included with other oxides in the initial glass batch to form a homogeneous glass melt. The dissolved nucleation agents subsequently precipitate at reduced temperatures because of strong oversaturation, i.e., via secondary phase separation of TiO_2 or ZrO_2 [18]. The precipitation is considered a homogeneous nucleation process which acts as an initiator for the crystallization of the remaining glass. In G18m, to which the TiO_2 was added as a separate phase, no TiO_2 was identified by XRD after the powders were heat-treated at 850 and 750 °C as shown in Fig. 5. The addition of TiO_2 to G18 glass seemed to promote more hexa-celsian phase ($BaAl_2Si_2O_8$) (Fig. 4B and D) and an additional phase of $Ba_2TiSi_2O_8$. Recalling from above that chemical analysis of the hybrid mica seal with G18 glass across the reacted regions showed different concentrations of Ba, it seems likely that the reduced reactivity of G18m compared to G18 glass with mica flakes was due to a lower Ba concentration in the residual glass. Overall, the fracture along the glass/Inconel600 interface or through the G18m glass interlayer was similar to that observed for the seal with G18 interlayers, and this seal also showed poor thermal cycle stability. The lower leak rate of 0.16 sccm cm^{-1} for G18m was likely due to a denser interlayer microstructure than that of G18 with leak rates of 0.32 sccm cm^{-1} and a porous microstructure.

For the hybrid mica seal with glass G6 interlayers, constant leak rates were obtained during ageing, and intact mica flakes were observed at the fracture surfaces after the test. These shining fracture surfaces indicated that the G6 glass interlayers were strongly bonded with the Inconel600 top fixture as well as the SS430 bottom substrate. This is somewhat unexpected due to very large CTE mismatch between

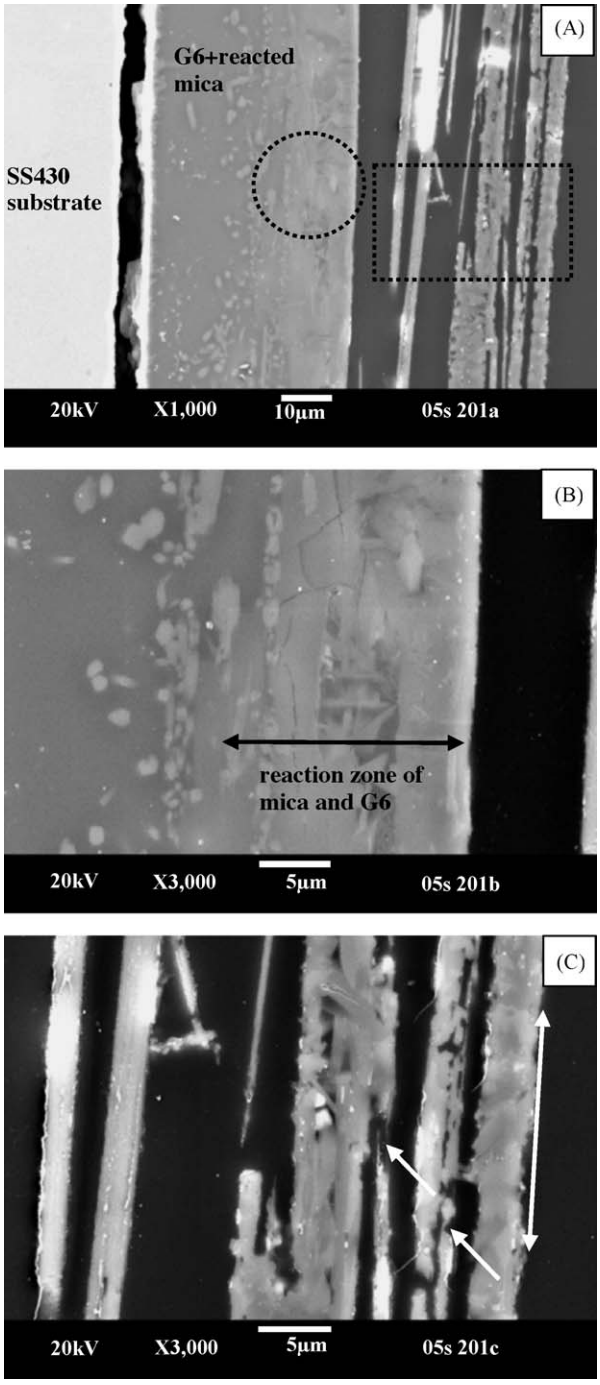

Fig. 13. Cross-section view of the hybrid phlogopite mica seal with G6 glass interlayers after ageing and thermal cycling: (A) an overall view, (B) and (C) are higher magnifications of the selected circle and rectangle area in (A). The different color contrast and microstructure features in (B) suggest that the mica layers close to the G6 glass may have reacted/melted with the glass to form a monolithic body. The arrows in (C) indicate further reaction of mica flakes with the G6 glass.

Inconel600 and the G6 glass, as well as between G6 and the SS430 substrate. One possible cause was that the G6 interlayers at the two interfaces were thinner, denser and had fewer microstructure defects, as shown in Fig. 13. The G6 thickness was ~30–40 μm while the thickness for G18 or G18m glass

interlayers was >140 μm. As a result, the glass interlayer did not fracture from the bonded surfaces (the crack between the glass interlayer and the SS430 substrate in Fig. 13A was likely formed by grinding and polishing during sample preparation). Although intact mica flakes were present on the fracture surfaces (Fig. 12C and D), the phlogopite mica did react to some extent with the G6 glass during the 508 h of ageing, as the mica flakes in direct contact with the G6 glass appeared to melt together with the G6 glass. The reaction zone was about 20–30 μm in thickness (arrow in Fig. 13B). EDS also confirmed about 8 times higher Mg content (from the mica) in the reaction zone than outside the zone. The central region of mica flakes was still somewhat degraded in that the mica showed roughened edges and some sections seemed dissolved away (arrows in Fig. 13C). Nevertheless, these degraded mica flakes still remained intact and may have provided some open channels for water vapor to exit rather than remaining trapped in the monolithic body, as appeared to be the case for the hybrid mica seal with G18 glass interlayers.

4. Conclusions

Three hybrid phlogopite mica seals were evaluated in a combined ageing and thermal cycling test. Three different glasses were used as interlayers: a standard Ba–Ca–Al silicate glass (G18), the same glass with 5 wt.% TiO_2 added (G18m), and a borosilicate glass (G6) which tended to remain vitreous. Samples were first aged at 800 °C for ~500 or ~1000 h in a simulated SOFC environment, followed by short-term thermal cycling. Hybrid mica seals with G18 glass interlayers showed extensive reaction and poor thermal cycle stability after ageing for 1036 h and 21 thermal cycles, with leak rates as high as 0.32 sccm cm^{-1}. Hybrid mica seals with G18m glass interlayers showed little or no reaction during ageing, but also poor thermal cycle stability with leak rates as high as 0.16 sccm cm^{-1}. Use of a borosilicate glass (G6) showed limited reaction with low leak rates during ageing (but was only tested for half as long) and very good thermal cycle stability with constant leak rates <0.01 sccm cm^{-1} over 56 thermal cycles. However, the glass has high alkali content and may not be suitable for long-term SOFC stack sealing applications. Fracture surface and microstructural analyses were also conducted. The fracture paths and degradation/reactions were discussed and found to be consistent with the leakage data during constant temperature ageing and subsequent thermal cycles.

Acknowledgements

The authors would like to thank S. Carlson for SEM sample preparation, and J. Coleman for SEM analysis. This paper was funded as part of the Solid-State Energy Conversion Alliance (SECA) Core Technology Program by the US Department of Energy's National Energy Technology Laboratory (NETL). Pacific Northwest National Laboratory is operated by Battelle Memorial Institute for the US Department of Energy under Contract no. DE-AC06-76RLO 1830.

References

[1] T. Yamamoto, H. Ito, M. Mori, N. Mori, T. Watanabe, Compatibility of mica glass-ceramics as gas-sealing materials for SOFC, Denki Kagaku 64 (6) (1996) 575–581.
[2] N. Lahl, D. Bahadur, K. Singh, L. Singheiser, K. Hilpert, Chemical interactions between aluminosilicate base sealants and the components on the anode side of solid oxide fuel cells, J. Electrochem. Soc. 149 (5) (2002) A607–A614.
[3] K. Ley, M. Krumpelt, J. Meiser, I. Bloom, Glass-ceramic sealants for solid oxide fuel cells. Part I. Physical properties, J. Mater. Res. 11 (6) (1996) 1489–1493.
[4] N. Lahl, K. Singh, L. Singheiser, K. Hilpert, Crystallization kinetics in $AO–Al_2O_3–SiO_2–B_2O_3$ glasses (A = Ba, Ca, Mg), J. Mater. Sci. 35 (2000) 3089–3096.
[5] Y.-S. Chou, J.W. Stevenson, L.A. Chick, Ultra-low leak rate of hybrid compressive mica seals for solid oxide fuel cells, J. Power Sources 112 (1) (2002) 130–136.
[6] Y.-S. Chou, J.W. Stevenson, L.A. Chick, Novel compressive mica seals with metallic interlayers for solid oxide fuel cell applications, J. Am. Ceram. Soc. 86 (6) (2003) 1003–1007.
[7] S. Simner, J.W. Stevenson, Compressive mica seals for SOFC applications, J. Power Sources 102 (1–2) (2001) 310–316.
[8] K.S. Weil, J.S. Hardy, J.Y. Kim, Use of a novel ceramic-to-metal braze for joining in high temperature electrochemical devices, Joining Adv. Specialty Mater. V 5 (2002) 47–55.
[9] Y.-S. Chou, J.W. Stevenson, Mid-term stability of novel mica-based compressive seals for solid oxide fuel cells, J. Power Sources 115 (2) (2003) 274–278.
[10] K.D. Meinhardt, L.R. Pederson, US Patent 6,430,966, 2002.
[11] Y.-S. Chou, J.W. Stevenson, Thermal cycling and degradation mechanisms of compressive mica-based seals for solid oxide fuel cells, J. Power Sources 112 (2) (2002) 376–383.
[12] Y.-S. Chou, J.W. Stevenson, Phlogopite mica-based compressive seals for solid oxide fuel cells: effect of mica thickness, J. Power Sources 124 (2) (2002) 473–478.
[13] Z. Yang, K.S. Weil, D.M. Paxton, J.W. Stevenson, Selection and evaluation of heat-resistant alloys for SOFC interconnect applications, J. Electrochem. Soc. 150 (9) (2003) A1188–A1201.
[14] H.C. Lin, W.R. Foster, Studies in the system $BaO–Al_2O_3–SiO_2$. I. The polymorphism of celsian, Am. Miner. 53 (1968) 134–144.
[15] D. Bahat, Kinetic study on the hexacelsian–celsian phase transformation, J. Mater. Sci. 53 (1968) 134–144.
[16] V.S.R. Murthy, M.H. Lewis, Matrix crystallization and interface structure in SiC–celsian composites, Br. Ceram. Trans. J. 89 (5) (1990) 173–174.
[17] R. Rice, Perspective on fractography, in: J.R. Varner, V.D. Frechette (Eds.), Fractography of Glasses and Ceramics, Advances in Ceramics, vol. 22, American Ceramic Society, 1986, pp. 3–56.
[18] W. Vogel, Chemistry of Glass, American Ceramic Society, 1985, p. 223.